Communication

Organic Nanotube with Subnanometer, pH-Responsive Lumen

Shawn M. Darnall, Changyi Li, Martha Dunbar, Marco A. Alsina, Sinan Keten, Brett A. Helms, and Ting Xu

J. Am. Chem. Soc., **Just Accepted Manuscript** • DOI: 10.1021/jacs.9b03732 • Publication Date (Web): 25 Jun 2019

Organic Nanotube with Subnanometer, pH-Responsive Lumen

Shawn M. Darnall,[†] Changyi Li,[‡] Martha Dunbar,[¶] Marco Alsina,[¶] Sinan Keten,[¶] Brett A. Helms,[*,‡] and Ting Xu[*,‡,†,§]

†*Department of Materials Science & Engineering, University of California, Berkeley, Berkeley, CA 94720, USA*

‡*The Molecular Foundry, Lawrence Berkeley National Laboratory, Berkeley, California 94720, USA*

¶*Department of Civil & Environmental Engineering and Mechanical Engineering, Northwestern University, Evanston, Illinois 60208, USA*

§*Department of Chemistry, University of California, Berkeley, Berkeley, CA 94720, USA*

Received June 6, 2019; E-mail: bahelms@lbl.gov; tingxu@berkeley.edu

Abstract: While many synthetic nanotubes with a hydrophobic lumen and fast molecular transport have been developed, decorating the interior of these channels with polar and/or responsive functional groups remains challenging. In transmembrane proteins like the aquaporin and M2 channels, the presence of histidine residues in a mostly hydrophobic channel has led to enhanced selectivity and pH-based activation. Herein, we report the synthesis of Bzim-CP, a cyclic octapeptide that contains a benzimidazole functionality as a chemical and structural mimic of histidine. Bzim-CP undergoes different protonation states, forms sub-nanometer nanotubes, and projects two different ionizable functionalities into the lumen. Present studies open up synthetic possibilities to functionalize sub-nm porous channels as basis toward understanding new transport phenomena.

Nanotubes are promising materials capable of fast separations with molecular sieving,[1–3] but obtaining enhanced separation properties relies on controlling their pore dimensions, size-dispersity, and interior chemical functionality.[2] Transmembrane proteins such as aquaporin[4] and the M2 channel[5] have well-defined channel interiors that include polar amino acids like histidine in a hydrophobic channel. These features enable exceptional selectivity, flux, and even stimuli-responsive behavior for the M2 channel and have inspired the design of many synthetic nanochannels.

Fully mimicking these structural and chemical properties synthetically has been nontrivial if not impossible. Carbon nanotubes[6–9] and pillarenes[10] have fast water transport due to confinement and their hydrophobic and smooth interior, but they are difficult to functionalize internally and control for size. Lyotropic liquid crystals self-assemble into three dimensional structures with interconnected, highly charged pores that separate molecules by polarity, charge, and size.[11,12] Although they have been macroscopically fabricated into desalination membranes, processing limitations and lack of a hydrophobic core limit water flux. Metal organic frameworks have pores with tunable chemistry and geometry that are promising for separations.[1,13] However, they can be difficult to incorporate into polymeric membranes because of materials compatibility issues.[14]

Self-assembling cyclic peptides (CP) can form high aspect ratio nanotubes (CPN) with subnanometer channels. They can mimic the hourglass shape of transmembrane channels[15] or be used to generate porous membranes with oriented channels.[16,17] Pore size,[18,19] shape,[20] and exterior chemical properties[21–23] can be precisely tuned by changing the number or type of the amino acids in the CP backbone, and recent efforts have focused on introducing new chemical functionality to the interior.[24] Hydrophobic features including a methyl group[20] and portions of cyclic rings have been introduced to the interior by using artificial amino acids.[25,26]

Introducing different polar or stimuli-responsive groups to the interior of the CPN is much more desirable to mimic natural channel proteins, but success is rather limited. The earliest example relied on a lipid environment to twist exterior polar groups into the interior.[27] Later, cyclic γ-residues were used to insert hydroxyl[28–30] and hemiaminalic oxygen[31] functionalities. The hydroxyl group, however, interacted with the backbone and limited assembly to spherical clusters rather than forming straight nanotubes which are preferred for separations. CPNs with fluorinated interiors were recently reported.[32] Considering the design of these different CPNs, in particular to maintain subnanometer channel diameters needed for size selection, there are many challenges to making CPNs with polar interiors. The main obstacles include eliminating unintended hydrogen bonds that prevent nanotube formation,[29] reducing side reactions, and cyclizing peptides with bulky protecting groups.

Herein, we report a CPN that contains a benzimidazole group in the backbone where each sub-unit projects one of two ionizable nitrogen groups to the interior. The structural and chemical similarity to histidine's imidazole group introduces pH-responsive properties to the CP.

Synthesis of the benzimidazole-containing CPN, Bzim-CP, is shown in Scheme 1 and started with synthesizing an artificial amino acid. To eliminate side reactions during the subsequent step, **1** was esterified and recrystallized in ethanol to produce **2** (62%). Boc protection of the aniline was performed using di-*tert*-butyl-dicarbonate and DMAP in toluene producing **3** (74%). The ester was subsequently hydrolyzed using NaOH in a water/ethanol mixture. After careful acidification, extraction, and recrystallization, **4** was obtained (68%). The nitro group was fully hydrogenated using H_2 and 5% Pd/C in methanol, affording **5** and used without further purification. Fmoc-protection of the aniline group was attempted using Fmoc-Cl and Fmoc-OSu but had low yield due to side reactions. Instead, protected dipeptide **6** was formed by synthesizing Fmoc-D-Ala-Cl and reacting it with **5** (61%).

Using SPPS on a 2-chlorotrityl chloride resin, linear peptide chain, H_2N-**6**-A-K-A-L-A-K-OH, was grown. (Underline denotes D-stereoisomer). The placement of dipeptide **6** in the sequence is important for CP cyclization and was systematically screened. The optimal location was at the end of

the growing chain. Placing it earlier also resulted in either premature cleavage from the resin or side reactions. The protected peptide was released from the resin using 1% trifluoroacetic acid (TFA) in DCM and cyclized using HATU. Other coupling agents (T3P, DIC/HOBt, HCTU, HBTU, PyBOP) were tested but had negligible yield. A final deprotection in TFA at 60°C resulted in a ring-closing reaction between **5** and the neighboring carbonyl, producing Bzim-CP. The product was purified by HPLC and characterized by LC-MS and NMR (SI3.1-3.4). NMR spectra indicate that both the exterior and interior nitrogens of the benzimidazole are bonded to hydrogen in equal likelihood (SI3.3).

Scheme 1. Synthesis of Bzim-CP

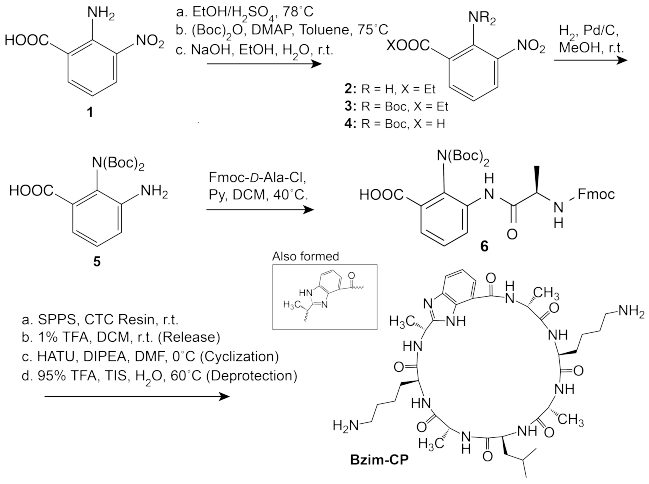

Individual CPs stack to form nanotubes through hydrogen bonds, resembling antiparallel β-sheets which can be measured by spectroscopy.[33] Nanotubes were drop-cast onto a CaF_2 plate, and their solid-state assembly behavior was probed by FTIR, Figure 1a. Bzim-CP strongly absorbed at 3272, 1632, and 1545 cm^{-1} which correspond to the Amide A (N−H stretching), Amide I (C=O stretching, perpendicular component), and Amide II (N−H bending and CN stretching) bands, respectively, and are indicative of β-sheets[34] and nanotube formation. The spectra is similar to and within a few cm^{-1} of other reported CPNs.[16,20,33] 1673 cm^{-1} is due to residual TFA from HPLC purification.[35]

Circular dichroism (CD) was used to study the assembly in solution, Figure 1b. Bzim-CP readily dissolved in 10 mM tris buffer (pH 7.4), methanol, and ethanol, and typical β-sheet signatures were measured with a peak and trough near 200 nm and 220 nm, respectively. This finding indicates that there is still a significant degree of nanotube formation despite hydrogen bond competition from the solvent. The slight differences in peak and trough locations suggest solvent-dependent changes in the CP stacking behavior or backbone configuration. Bzim-CP, however, did not dissolve in acetonitrile even at concentrations down to 1 μM, but a 40 μM suspension did show β-sheet-like signature with an offset trough. Crystallization of Bzim-CP was attempted to probe the differences in stacking behavior but was unsuccessful.

Bzim-CP was compared to two variants, (i) $(K\underline{A})_4$-CP[17] which contains only α-amino acids and (ii) Mba-CP[20] which uses a γ-amino acid for interior methylation, Figure 1c and 1d. In methanol, the spectra for Bzim-CP had similar peak and trough wavelengths as that for $(K\underline{A})_4$-CP, although intensities varied and suggests different degrees of nanotube formation. Surprisingly, the spectra for Bzim-CP and Mba-

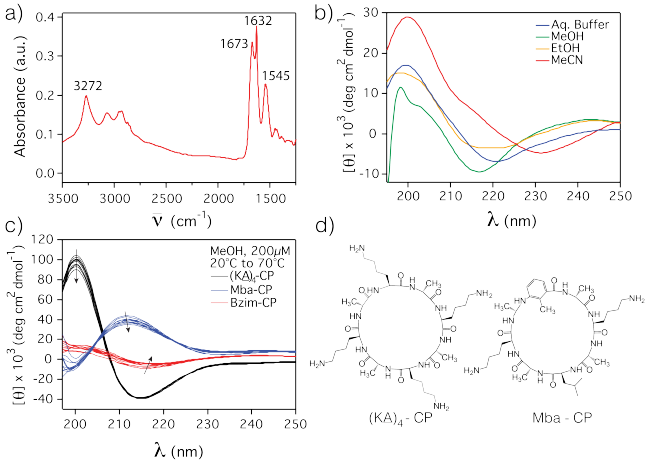

Figure 1. a) FT-IR spectra of dried Bzim-CP nanotubes. b) Circular dichroism spectra of Bzim-CP in 10 mM tris buffer, pH 7.4 and organic solvents. MeCN samples were taken as a suspension. c) Temperature dependence of Bzim-CP and the two CPN variants shown in (d).

CP differed greatly despite both containing aromatic compounds, with Mba-CP lacking β-sheet signatures. Each solution was also heated from 20°C to 65°C, and the overall curve shapes were maintained, indicating thermal stability of the CPNs. The peaks for $(K\underline{A})_4$-CP and Mba-CP showed a 14% and 21% decrease, respectively, in intensity while Bzim-CP showed an overall upward shift. In acetonitrile, $(K\underline{A})_4$-CP also did not dissolve, but Mba-CP did at 100 μM and its spectra suggests nanotube formation as reported previously.[20] Considering their relative solubilities and CD spectra in the different solvents, $(K\underline{A})_4$-CP likely has the greatest ability to form nanotubes, followed by Bzim-CP.

Molecular dynamics simulations were performed to further study the in-solution equilibrium assembly behavior of Bzim-CP nanotubes. Toluene, a low dielectric solvent, was used to strongly encourage hydrogen bonding between CPs for nanotube formation, Figure 2 and SI4. Bzim-CP formed

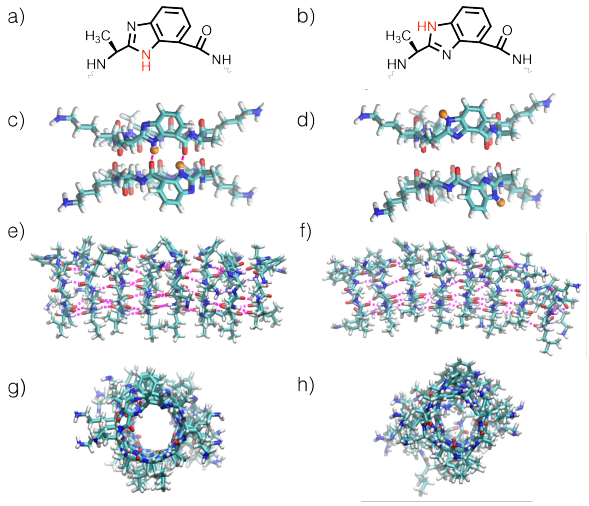

Figure 2. MD simulations of Bzim-CP assembly in toluene depending on whether N−H is on interior (a,c,e,f) or exterior (b,d,f,h). a,b) The respective chemical structure. c,d) Dimer formation with hydrogen bond formation between benzimidazoles highlighted in (c) in pink. e-h) Side and cross-sectional views of nanotubes.

fewer inter-ring bonds than (KA)$_4$-CP, which is consistent with its weaker CD signal. The ring-stacking behavior was also found to be dependent on which nitrogen on the benzimidazole was protonated. When the lumen contains the hydrogen, the N−H group aligns well with the carbonyl on the neighboring ring, allowing on average 6.4 hydrogen bonds to form between neighboring CPs, Figure 2c and 2e. Straight nanotubes are formed, which is ideal for transport. However, when N−H is located on the exterior of the nanotube, the same alignment cannot occur, resulting in only 5.3 hydrogen bonds forming. To compensate, the CPN bends to increase inter-ring interactions, Figure 2d and 2f. The side and cross-sectional views give further insight into the backbone configuration and the stacking behavior. The benzimidazole group splays off at an angle instead of lying flat in the ring. Hydrogen bonding is maximized by stacking the CPs in an antiparallel fashion, where the benzimidazole group in adjacent rings angle in the opposite directions.

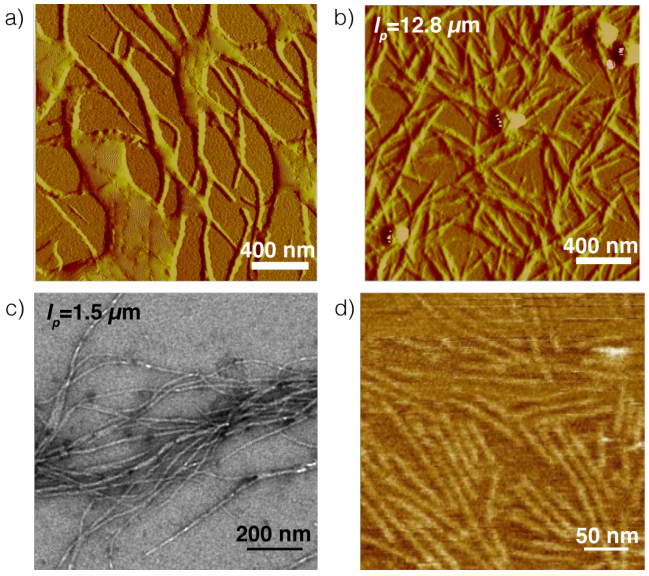

Figure 3. AFM of Bzim-CP nanotube bundles cast from (a) toluene and (b) DMF. (c) TEM of Bzim-CP cast from acetonitrile. (d) AFM of PEG-conjugated Bzim-CP cast from DMF. l_p is the measured persistence length.

Dried Bzim-CP nanotubes were visualized as final confirmation of assembly, Figure 3. Using atomic force microscopy, samples spun-cast from toluene were observed as large, networked bundles of nanotubes. In contrast, Bzim-CP cast from dimethylformamide formed straight nanotube bundles measuring 583 ± 390 nm long and 30 ± 7 nm wide. Bzim-CP in acetonitrile was drop-cast onto a carbon grid and negatively stained for TEM imaging. Highly curved, entangled bundles measuring 482 ± 310 nm long and 14 ± 2 nm wide were observed. The various degrees of bundling between the samples likely resulted from both differences in the hydrophobic effect in solution as well as a hierarchically-oriented alignment driven by the local concentrations of nanotubes upon drying.[36,37] Due to the apparent differences in curvature, the persistence lengths, l_p, were approximated by comparing contour lengths and end-to-end distances of the bundles (SI3.8). The l_p of samples cast from DMF were 8.4x longer than those from acetonitrile. Errors associated with measuring their diameters made comparing bending moduli difficult, but differences in diameters likely caused the observed differences. For dispersion and future integration into polymer films, poly(ethylene glycol) (MW = 2000 g/mol) was conjugated to the exterior lysine handles. The CPN-PEG conjugates were cast from dimethylformamide, resulting in shorter and narrower individual nanotubes measuring 121 ± 56 nm long and 7 ± 1 nm wide.

The change in electronic structure of the Bzim-CP backbone was monitored as a function of pH using UV-Vis spectroscopy, Figures 4a and 4b. At pH 2.1, an absorbance peak and shoulder at 250 nm and 280 nm, respectively, were observed. With increasing pH, the absorption peak and shoulder shifted to 270 nm and 300 nm, respectively, before becoming a single peak at 315 nm, revealing three protonation states with pKa values of approximately 3.2 and 11.5. Reversing the pH showed that the absorption change is reversible. Loss of the β-sheet signal was observed by CD as the pH was decreased below the lower pKa, Figure 4c. The normalized signal at 220 nm correlated strongly with the protonation states predicted by the Hendersen-Hasselbalch equation, suggesting that the CPN disassembles due to ionic repulsion from the positively charged benimidazole groups. Due to high absorbance, this process could not be repeated near the higher pKa but is expected to be similar as Bzim-CP becomes negatively charged. (KA)$_4$-CP and Mba-CP showed no pH dependence under the same conditions because they have no ionizable backbone groups in this pH range (SI3.5). While Bzim-CP dissociates in solution at extreme pHs, putting Bzim-CP in a condensed phase like a polymer matrix may help maintain the structure, and further stabilization may be possible by doping in other CPs into the nanotube to separate charged CPs.[38,39] The latter approach would also better mimic the chemical makeup found in protein channels.

To conclude, we have developed an organic nanotube that introduces new pH-responsive properties into the interior of the channel, and its polymer conjugate should be amenable to subnanometer porous film fabrication.[17] Because the benzimidazole functionality mimics histidine side chains, Bzim-CP may introduce new biomimetic transport properties such as those found in transmembrane channels, and future work will focus on closely studying how the different interior prop-

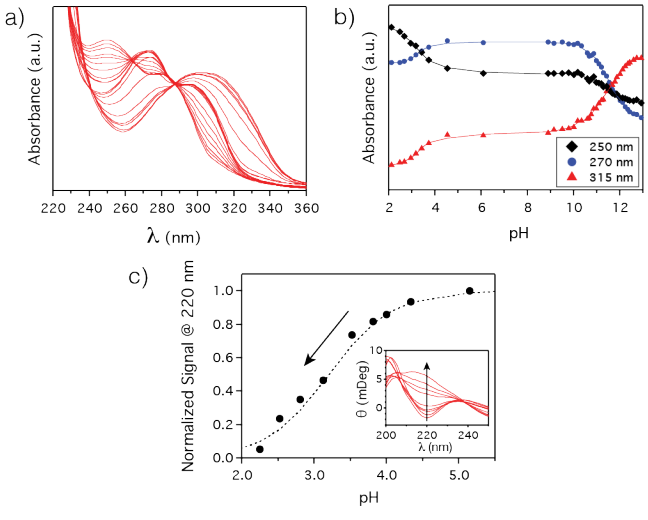

Figure 4. The changes in (a) absorption and (b) intensity of major peaks of Bzim-CP as a function of pH, revealing three ionization states. (c) Normalized CD signal (dots) compared to nonprotonated/protonated ratio predicted by the Henderson-Hasselbalch equation (dotted line) as a function of pH. Inset: corresponding CD spectrum, suggesting CPN dissociation

erties affect transport. The CPN in this work complements the already existing library of hydrophobic CPNs, bringing the field one step closer to achieving organic nanotubes with variable and dynamic interiors for better molecular recognition and transport.

Acknowledgement

This research was supported through the Center for Gas Separations Relevant to Clean Energy Technologies, an Energy Frontier Research Center funded by the US Department of Energy, Office of Science, Office of Basic Energy Sciences under Award DE-SC0001015. Portions of the work -including dipeptide 6 synthesis, CP synthesis, and tandem deprotection and Bzim cyclization- were carried out at the Molecular Foundry, which is supported by the Office of Science, Office of Basic Energy Sciences, of the U.S. Department of Energy under Contract No. DE-AC02-05CH11231. We also acknowledge the support of the Office of Naval Research (Grant # N00014-13-1-0760) and the National Science Foundation's Designing Materials to Revolutionize and Engineer our Future (DMREF) Award CBET-1234305.

Supporting Information Available

Experimental procedures and characterization data for all new compounds.

References

(1) Galizia, M.; Chi, W. S.; Smith, Z. P.; Merkel, T. C.; Baker, R. W.; Freeman, B. D. 50th Anniversary Perspective: Polymers and Mixed Matrix Membranes for Gas and Vapor Separation: A Review and Prospective Opportunities. *Macromolecules* **2017**, *50*, 7809–7843.

(2) Gin, D. L.; Noble, R. D. Designing the Next Generation of Chemical Separation Membranes. *Science; Science* **2011**, *332*, 674.

(3) Sianipar, M.; Kim, S. H.; Khoiruddin,; Iskandar, F.; Wenten, I. G. Functionalized carbon nanotube (CNT) membrane: progress and challenges. *RSC Adv.* **2017**, *7*, 51175–51198.

(4) Murata, K.; Mitsuoka, K.; Hirai, T.; Walz, T.; Agre, P.; Heymann, J. B.; Engel, A.; Fujiyoshi, Y. Structural determinants of water permeation through aquaporin-1. *Nature* **2000**, *407*, 599.

(5) Leiding, T.; Wang, J.; Martinsson, J.; DeGrado, W. F.; rskld, S. P. Proton and cation transport activity of the M2 proton channel from influenza A virus. *Proceedings of the National Academy of Sciences* **2010**, *107*, 15409.

(6) Holt, J. K.; Park, H. G.; Wang, Y.; Stadermann, M.; Artyukhin, A. B.; Grigoropoulos, C. P.; Noy, A.; Bakajin, O. Fast Mass Transport Through Sub-2-Nanometer Carbon Nanotubes. *Science; Science* **2006**, *312*, 1034.

(7) Hinds, B. J.; Chopra, N.; Rantell, T.; Andrews, R.; Gavalas, V.; Bachas, L. G. Aligned Multiwalled Carbon Nanotube Membranes. *Science; Science* **2004**, *303*, 62.

(8) Tunuguntla, R. H.; Allen, F. I.; Kim, K.; Belliveau, A.; Noy, A. Ultrafast proton transport in sub-1-nm diameter carbon nanotube porins. *Nat Nano* **2016**, *11*, 639–644.

(9) Tunuguntla, R. H.; Henley, R. Y.; Yao, Y.-C.; Pham, T. A.; Wanunu, M.; Noy, A. Enhanced water permeability and tunable ion selectivity in subnanometer carbon nanotube porins. *Science* **2017**, *357*, 792–796.

(10) Shen, Y.-x.; Si, W.; Erbakan, M.; Decker, K.; De Zorzi, R.; Saboe, P. O.; Kang, Y. J.; Majd, S.; Butler, P. J.; Walz, T.; Aksimentiev, A.; Hou, J.-l.; Kumar, M. Highly permeable artificial water channels that can self-assemble into two-dimensional arrays. *Proceedings of the National Academy of Sciences* **2015**, *112*, 9810–9815.

(11) Hatakeyama, E. S.; Gabriel, C. J.; Wiesenauer, B. R.; Lohr, J. L.; Zhou, M.; Noble, R. D.; Gin, D. L. Water filtration performance of a lyotropic liquid crystal polymer membrane with uniform, sub-1-nm pores. *Journal of Membrane Science* **2011**, *366*, 62 – 72.

(12) Wiesenauer, B. R.; Gin, D. L. Nanoporous polymer materials based on self-organized, bicontinuous cubic lyotropic liquid crystal assemblies and their applications. *Polymer Journal* **2012**, *44*, 461.

(13) Zhang, H.; Hou, J.; Hu, Y.; Wang, P.; Ou, R.; Jiang, L.; Liu, J. Z.; Freeman, B. D.; Hill, A. J.; Wang, H. Ultrafast selective transport of alkali metal ions in metal organic frameworks with subnanometer pores. *Science Advances* **2018**, *4*.

(14) Semino, R.; Moreton, J. C.; Ramsahye, N. A.; Cohen, S. M.; Maurin, G. Understanding the origins of metalorganic framework/polymer compatibility. *Chemical Science* **2018**, *9*, 315–324.

(15) Fuertes, A.; Ozores, H. L.; Amorn, M.; Granja, J. R. Self-assembling Venturi-like peptide nanotubes. *Nanoscale* **2017**, *9*, 748–753.

(16) Ghadiri, M. R.; Granja, J. R.; Milligan, R. A.; McRee, D. E.; Khazanovich, N. Self-assembling organic nanotubes based on a cyclic peptide architecture. *Nature* **1993**, *366*, 324–327.

(17) Xu, T.; Zhao, N.; Ren, F.; Hourani, R.; Lee, M. T.; Shu, J. Y.; Mao, S.; Helms, B. A. Subnanometer Porous Thin Films by the Co-assembly of Nanotube Subunits and Block Copolymers. *ACS Nano* **2011**, *5*, 1376–1384.

(18) Khazanovich, N.; Granja, J. R.; McRee, D. E.; Milligan, R. A.; Ghadiri, M. R. Nanoscale Tubular Ensembles with Specified Internal Diameters. Design of a Self-Assembled Nanotube with a 13-Å Pore. *Journal of the American Chemical Society* **1994**, *116*, 6011–6012.

(19) Granja, J. R.; Ghadiri, M. R. Channel-Mediated Transport of Glucose across Lipid Bilayers. *Journal of the American Chemical Society* **1994**, *116*, 10785–10786.

(20) Hourani, R.; Zhang, C.; van, d. W.; Ruiz, L.; Li, C.; Keten, S.; Helms, B. A.; Xu, T. Processable Cyclic Peptide Nanotubes with Tunable Interiors. *Journal of the American Chemical Society* **2011**, *133*, 15296–15299.

(21) Fernandez-Lopez, S.; Kim, H.-S.; Choi, E. C.; Delgado, M.; Granja, J. R.; Khasanov, A.; Kraehenbuehl, K.; Long, G.; Weinberger, D. A.; Wilcoxen, K. M.; Ghadiri, M. R. Antibacterial agents based on the cyclic d,l--peptide architecture. *Nature* **2001**, *412*, 452.

(22) Ghadiri, M. R.; Granja, J. R.; Buehler, L. K. Artificial transmembrane ion channels from self-assembling peptide nanotubes. *Nature* **1994**, *369*, 301–304.

(23) Danial, M.; Perrier, S.; Jolliffe, K. A. Effect of the amino acid composition of cyclic peptides on their self-assembly in lipid bilayers. *Organic & Biomolecular Chemistry* **2015**, *13*, 2464–2473.

(24) Rodríguez-Vázquez, N.; Amorín, M.; Granja, J. R. Recent advances in controlling the internal and external properties of self-assembling cyclic peptide nanotubes and dimers. *Organic & Biomolecular Chemistry* **2017**, *15*, 4490–4505.

(25) Kubik, S. Large Increase in Cation Binding Affinity of Artificial Cyclopeptide Receptors by an Allosteric Effect. *Journal of the American Chemical Society* **1999**, *121*, 5846–5855.

(26) Amorín, M.; Castedo, L.; Granja, J. R. New Cyclic Peptide Assemblies with Hydrophobic Cavities: The Structural and Thermodynamic Basis of a New Class of Peptide Nanotubes. *Journal of the American Chemical Society* **2003**, *125*, 2844–2845.

(27) Wang, D.; Guo, L.; Zhang, J.; Roeske, R. W.; Jones, L. R.; Chen, Z.; Pritchard, C. Artificial ion channels formed by a synthetic cyclic peptide. *The Journal of Peptide Research* **2001**, *57*, 301–306.

(28) Reiriz, C.; Amorín, M.; Garcia-Fandino, R.; Castedo, L.; Granja, J. R. α,γ-Cyclic peptide ensembles with a hydroxylated cavity. *Organic & Biomolecular Chemistry* **2009**, *7*, 4358–4361.

(29) Rodríguez-Vázquez, N.; Garcia-Fandino, R.; Amorín, M.; Granja, J. R. Self-assembling α,γ-cyclic peptides that generate cavities with tunable properties. *Chemical Science; Chem.Sci.* **2016**, *7*, 183–187.

(30) Rodríguez-Vázquez, N.; Amorín, M.; Alfonso, I.; Granja, J. R. Anion Recognition and Induced Self-Assembly of an α,γ-Cyclic Peptide To Form Spherical Clusters. *Angewandte Chemie International Edition* **2016**, *55*, 4504–4508.

(31) Guerra, A.; Brea, R. J.; Amorín, M.; Castedo, L.; Granja, J. R. Self-assembling properties of all γ-cyclic peptides containing sugar amino acid residues. *Organic & Biomolecular Chemistry* **2012**, *10*, 8762–8766.

(32) Burade, S. S.; Saha, T.; Bhuma, N.; Kumbhar, N.; Kotmale, A.; Rajamohanan, P. R.; Gonnade, R. G.; Talukdar, P.; Dhavale, D. D. Self-Assembly of Fluorinated Sugar Amino Acid Derived α, γ-Cyclic Peptides into Transmembrane Anion Transport. *Organic Letters* **2017**, *19*, 5948–5951.

(33) Kim, H. S.; Hartgerink, J. D.; Ghadiri, M. R. Oriented Self-Assembly of Cyclic Peptide Nanotubes in Lipid Membranes. *Journal of the American Chemical Society* **1998**, *120*, 4417–4424.

(34) Miyazawa, T.; Blout, E. R. The Infrared Spectra of Polypeptides in Various Conformations: Amide I and II Bands1. *Journal of the American Chemical Society* **1961**, *83*, 712–719.

(35) Haris, P. I.; Chapman, D. The conformational analysis of peptides using fourier transform IR spectroscopy. *Biopolymers* **1995**, *37*, 251–263.

(36) Liu, K.; Xing, R.; Chen, C.; Shen, G.; Yan, L.; Zou, Q.; Ma, G.; Mhwald, H.; Yan, X. Peptide-Induced Hierarchical Long-Range Order and Photocatalytic Activity of Porphyrin Assemblies. *Angewandte Chemie International Edition* **2015**, *54*, 500–505.

(37) Wang, J.; Liu, K.; Xing, R.; Yan, X. Peptide self-assembly: thermodynamics and kinetics. *Chem. Soc. Rev.* **2016**, *45*, 5589–5604.

(38) Brea, R. J.; Vázquez, M. E.; Mosquera, M.; Castedo, L.;

Granja, J. R. Controlling Multiple Fluorescent Signal Output in Cyclic Peptide-Based Supramolecular Systems. *Journal of the American Chemical Society* **2007**, *129*, 1653–1657.

(39) Rho, J. Y.; Brendel, J. C.; MacFarlane, L. R.; Mansfield, E. D. H.; Peltier, R.; Rogers, S.; Hartlieb, M.; Perrier, S. Probing the Dynamic Nature of SelfAssembling Cyclic PeptidePolymer Nanotubes in Solution and in Mammalian Cells. *Advanced Functional Materials* **2018**, *28*.

Graphical TOC Entry